

Axisymmetric flows in Hall-MHD: A tendency towards finite-time singularity formation

Jürgen Dreher,^{1,*} Viktor Ruban,^{2,†} and Rainer Grauer^{1,‡}

¹*Theoretische Physik I, Ruhr-Universität Bochum, Germany*

²*Landau Institute for Theoretical Physics, Moscow, Russia*

(Dated: May 24, 2005)

Abstract

Spontaneous development of shock-like singularities in axisymmetric solutions of the Hall-MHD equations is discussed. It is shown that the Hall-term in Ohm's law leads to a Burgers-type equation for the magnetic field evolution in weakly compressible regime. Numerical simulations are used to investigate the validity of this approximation for a particular class of initial conditions.

PACS numbers: 52.30.-q, 52.65.-y, 52.30.Ex, 52.65.Kj

*Electronic address: dreher@tp1.rub.de

†Electronic address: ruban@itp.ac.ru

‡Electronic address: grauer@tp1.rub.de

I. INTRODUCTION

The problem of spontaneous formation of singular nonlinear structures in fluids and plasmas has attracted efforts of many researchers over the last two decades. For instance, besides from being a fascinating open mathematical challenge [1–6] singular structures play a dominant role in understanding intermittency in strong turbulent systems. This is manifested in phenomenological models of fluid and plasma turbulence [7–10] as well as in the high order statistics in Burgers turbulence [11–13]. A further example of the importance of nearly singular structures is fast magnetic reconnection in collisionless plasmas: It is now widely accepted [14, 15] that terms in Ohm’s law that are beyond the ideal MHD model, like the Hall term and electron inertia, produce a Petschek-like configuration [16] where a localized x-point structure in combination with the Hall dynamics is responsible for fast reconnection rates.

Without solving the formation of singular structures and analysing their geometry, our understanding of many properties of these systems remains incomplete. However, dynamical mechanisms for singularities and corresponding small-scale structures are different in different physical models. Below we consider a magnetized plasma, where the most important singular structures are current sheets (see [6, 14, 17] and references therein). The tendency towards current sheet formation in plasmas can be explained already in the frame of relatively simple models as the ideal Electron Magnetohydrodynamics (EMHD) [18–21], which is known to be a particular simplified case of the more general two-fluid plasma model [20, 22]. Particularly simple is the situation of axisymmetric EMHD-flows and a purely azimuthal magnetic field. Here, the system is described by a single scalar function related to the frozen-in generalized electron vorticity [18, 20] which depends only on the radial coordinate, the axial coordinate, and time. It’s evolution is determined by a nonlinear transport equation, which reduces to the well known Burgers equation in the limit of vanishing electron mass, while the generalized electron vorticity in this limit coincides with the magnetic field [18, 20]. Typical solutions of that nonlinear equation exhibit formation of a shock-like gradient type singularity in the magnetic field after a finite time that corresponds to the axial cross-section of a current sheet. Further development of the shock is governed both by dissipation (finite resistivity and viscosity) and by nonlocal effects due to finite electron mass [18, 20, 21].

As these results from EMHD implicitly treat the ion component as an immobile background, one obvious question is whether, and how, the dynamical ion response would alter the tendency of current sheet formation in these settings. To address this question, we start from the ideal Hall-MHD model, i.e. taken into account the ion motion, but neglecting the effect of electron inertia. In order to connect these new investigations to the previous work, we will first start with the special case of a reduced system with known analytical solution similar to the case described above. This serves to identify the fundamental underlying mechanism responsible for the singularity formation as well as a test for the sophisticated numerical treatment using block-structured adaptive mesh refinement [23] which is necessary to resolve the small scale structures. From these comparison, we could gain enough confidence in the numerical method to draw conclusions for the general case with mobile ions and answer the question whether or not the ion response might prevent or inhibit the current sheet formation.

II. THEORY

The equations of ideal Hall-MHD for the plasma mass density ρ , the ion velocity \mathbf{u} , and the magnetic field \mathbf{b} can be written as follows

$$\frac{\partial \rho}{\partial t} = -\text{div}(\rho \mathbf{u}), \quad (1)$$

$$\frac{\partial \mathbf{u}}{\partial t} = [\mathbf{u} \times \text{curl} \mathbf{u}] + \frac{1}{\rho} [\text{curl} \mathbf{b} \times \mathbf{b}] - \nabla \left(\frac{\mathbf{u}^2}{2} + w(\rho) \right), \quad (2)$$

$$\frac{\partial \mathbf{b}}{\partial t} = \text{curl} \left[\left(\mathbf{u} - \frac{d_i}{\rho} \text{curl} \mathbf{b} \right) \times \mathbf{b} \right], \quad (3)$$

where d_i is the ion inertial length, and $w(\rho)$ is a known function determined by the thermal pressure $p(\rho)$, such that $dw = dp/\rho$ (we consider either isentropic or isothermal flows). The above system admits axisymmetric solutions of the form $\rho = \rho(z, r, t)$, $\mathbf{u} = \mathbf{e}_z U(z, r, t) + \mathbf{e}_r V(z, r, t)$, and $\mathbf{b} = \mathbf{e}_\varphi B(z, r, t) =: -\mathbf{e}_\varphi r \rho(z, r, t) \beta(z, r, t)$, where z, r, φ are cylindrical coordinates with unit vectors $\mathbf{e}_z, \mathbf{e}_r, \mathbf{e}_\varphi$. Let us also consider the generalized ion vorticity

$$\boldsymbol{\Omega} = \text{curl} \mathbf{u} + d_i^{-1} \mathbf{b} =: \mathbf{e}_\varphi r \rho(z, r, t) \alpha(z, r, t). \quad (4)$$

It is easily seen that the field $\mathbf{\Omega}$ is frozen-in into the ion fluid, since the equation of motion for $\mathbf{\Omega}$ is

$$\frac{\partial \mathbf{\Omega}}{\partial t} = \text{curl}[\mathbf{u} \times \mathbf{\Omega}]. \quad (5)$$

The above introduced functions α and β possess important properties. Indeed, we can easily obtain from Eqs.(1-3) that

$$\frac{\partial \rho}{\partial t} + \frac{1}{r} \frac{\partial}{\partial r}(rV\rho) + \frac{\partial}{\partial z}(U\rho) = 0, \quad (6)$$

$$\frac{\partial V}{\partial z} - \frac{\partial U}{\partial r} = r\rho(\alpha + d_i^{-1}\beta), \quad (7)$$

$$\frac{\partial \alpha}{\partial t} + U \frac{\partial \alpha}{\partial z} + V \frac{\partial \alpha}{\partial r} = 0, \quad (8)$$

$$\frac{\partial \beta}{\partial t} + U \frac{\partial \beta}{\partial z} + V \frac{\partial \beta}{\partial r} + 2d_i\beta \frac{\partial \beta}{\partial z} + d_i \frac{r\beta}{\rho} \left(\frac{\partial \rho}{\partial r} \frac{\partial \beta}{\partial z} - \frac{\partial \rho}{\partial z} \frac{\partial \beta}{\partial r} \right) = 0. \quad (9)$$

For brevity, below we use the subscripts t, z, r to denote the corresponding partial derivatives of unknown functions. Eq.(8) implies that function α remains constant along the trajectories determined by the ion velocity field $\mathbf{e}_z U + \mathbf{e}_r V$. Analogously, from Eq.(9) it follows that function β is transported by another vector field,

$$\mathbf{F} = \mathbf{e}_z[U + d_i\beta(2 + r\rho_r/\rho)] + \mathbf{e}_r[V - d_i\beta r\rho_z/\rho]. \quad (10)$$

Thus, the time evolution of the functions α and β is nothing else but just a motion of their levels in z - r plane. Therefore, once bounded initially, these functions cannot grow at later times. However, their gradients are allowed to increase significantly. From this point of view, Eq.(9) deserves particular attention due to the term $2d_i\beta\beta_z$, which produces a permanent tendency towards shock formation in β -profile. Very obviously this tendency is manifested in a region near the z -axis ($r \rightarrow 0$), where the dominant terms in Eq.(9) are

$$\beta_t + U\beta_z + 2d_i\beta\beta_z = 0. \quad (11)$$

Except for the term $U\beta_z$, this is the well-known Burgers equation. For the quantity $q = -\beta_z$ we have from Eq.(11) a remarkable equation

$$\dot{q} = -qU_z + 2d_iq^2, \quad (12)$$

where $\dot{q} \equiv q_t + (U + 2d_i\beta)q_z$ is the total (or convective) derivative along trajectories determined by the field \mathbf{F} on the axis. Eq.(12) can be easily solved along each particular

trajectory,

$$q(t) = q(0)e^{-A(t)} \left[1 - 2d_i q(0) \int_0^t e^{-A(\tau)} d\tau \right]^{-1}, \quad (13)$$

where $A(t)$ is defined as the time integral of U_z on that trajectory,

$$A(t) \equiv \int_0^t U_z(t_1) dt_1. \quad (14)$$

These formulas clearly give us a finite-time singularity with $\max(q) \sim (t^* - t)^{-1}$, provided that $q(0) > 0$ and $U_z < 0$ (then, the term with U acts to accelerate the shock formation). However, the singularity is still possible when U_z is positive but sufficiently small. For instance, with globally bounded $U_z < C$ the singularity definitely takes place if $2d_i \max(q(0)) > C$.

For simplicity, we have considered above the case $r \rightarrow 0$, but actually shocks can also develop at $r \neq 0$ if only the term $2d_i \beta \beta_z$ locally dominates the other terms in Eq.(9) containing spatial derivatives β_z and β_r . The last term in Eq.(9) is a cross product, and therefore is of less importance in typical situations when the gradients $\nabla \rho$ and $\nabla \beta$ have almost the same direction in a singular domain. Most important terms, that can in general prevent the shock formation, are the convective terms $U\beta_z + V\beta_r$. However, if the gradients ∇U and ∇V remain bounded, the convective terms cannot stop singularity, provided $\max(q(0))$ is large enough. Indeed, this situation can be found in the weakly compressible limit, when $|\mathbf{u}|$ and $|\mathbf{b}|$ are small compared to the speed of sound c_s , and relative variations of the density are small. In this case the weak compressibility condition $\rho \approx 1$ makes the ion velocity field \mathbf{u} nearly divergence-free. Therefore, taking into account Eq.(7), for localized structures we may conclude that the spatial derivatives of U and V are finite:

$$|\nabla U|, |\nabla V| \sim l(\alpha + d_i^{-1}\beta),$$

where l is a constant characteristic length given by an initial state, and α and β are some typical initial absolute values. Thus, having estimated different terms in Eq.(9), we naturally suggest for this case the hypothesis that the evolution of the system will move towards finite-time singularity formation, at least if the (rather strong) condition

$$l^2(\alpha + d_i^{-1}\beta) \lesssim d_i \beta \quad (15)$$

was initially satisfied. In particular, one may take

$$l \lesssim d_i, \quad \alpha \lesssim d_i^{-1}\beta \quad (16)$$

and expect the singularity. However, in our simulations we actually observed singularity even with $d_i < l$, when the necessary for shock formation condition

$$l(\alpha + d_i^{-1}\beta) \lesssim d_i \max(q), \quad (17)$$

was not satisfied at $t = 0$, but it was spontaneously achieved after some preliminary stage of evolution when $\max(q)$ increased just weakly (see numerical results below).

III. NUMERICAL SIMULATIONS

The above hypothesis has been tested by means of direct numerical simulations with a two-dimensional Hall-MHD code in cylindrical coordinates (z, r) . Integration is carried out with an explicit Runge-Kutta method and a fourth-order finite difference discretization on an adaptively refined mesh (AMR) with block structure [23]. This technique allows, at moderate computational costs, an efficient high-resolution coverage of the localized thin current sheets that are expected to form from the theoretical considerations in the previous section.

For the simulation runs discussed below, the mesh resolution, which is controlled by measuring the gradient scale of the magnetic field, typically varied between an equivalent of 256^2 points in smooth regions and $32\,768^2$ points at the location of the singularity formation. The latter corresponds to a grid spacing in z -direction of $\delta z = 1.2 \cdot 10^{-4}$. Due to the quadratic whistler dispersion, a drastic reduction of the integration time step is required under grid refinement in order to keep the numerical scheme stable, and this stability condition lead to values of the order of $\delta t \approx 10^{-7}$ in the late stage of the simulations. With up to 10^6 steps in a simulation, a run takes about 4 days on 4 AMD Opteron CPU's.

In order to stabilize the numerical scheme, an artificial hyper-diffusion term has been added to the equations for the magnetic field and the velocity. This consists of the operator $-a_\delta \Delta^2$, i.e. the Laplacian squared and scaled with an amplitude a_δ which in turn depends on the local grid spacing δ as $a_\delta = \nu \delta^2$. Therefore, a_δ differs between grid blocks of different resolution δ , and the entire operator has the same scaling $\propto (\delta)^{-2}$ as the Hall term, leading to a consistent stabilization of high-frequency discretization errors on all refinement levels. Its global magnitude ν was chosen such that $a_\delta = 3.5 \cdot 10^{-7}$ on the coarsest grid blocks and correspondingly smaller on finer blocks.

Equations (1)–(3) have been closed by the adiabatic plasma pressure $w(\rho) = \rho^2$, and the particular class of initial conditions for time $t = 0$,

$$\rho_0(z, r) = 1 \quad (18)$$

$$U_0(z, r) = \hat{v}(1 - r^2/2b^2)e^{-z^2/2a^2 - r^2/2b^2} \quad (19)$$

$$V_0(z, r) = \hat{v}(rz/2a^2)e^{-z^2/2a^2 - r^2/2b^2} \quad (20)$$

$$\beta_0(z, r) = [(a^2 - z^2)/2a^4 + (4b^2 - r^2)/2b^4] e^{-z^2/2a^2 - r^2/2b^2} \quad (21)$$

was used. Here, the exponential function localizes all quantities except ρ around $z = 0$, $r = 0$ on length scales a and b , respectively, and the parameter \hat{v} determines the initial amplitude for the plasma velocity, which is an incompressible poloidal flow around the magnetic field torus. It is easily seen that the particular choice $\hat{v}d_i = 1$ corresponds to a configuration without ion vorticity, $\alpha = 0$, and, as a consequence, the second condition in (16) for singularity formation is always fulfilled in this case. All simulations employed $a = b = 1/2$, and the remaining parameters that have been varied in the simulation are the normalized ion skin depth, d_i , and the amplitude of the initial ion velocity, \hat{v} .

Below, we will discuss results from two sets of simulations which use different values of the remaining parameters d_i and \hat{v} : The first one is taken with fixed $d_i = 0.2$ and $\hat{v} = -5, 0, 5$, respectively. In the second set, the ion inertial length is varied between $d_i = 0, 0.05, 0.2$ while the velocity amplitude \hat{v} is kept fixed to zero. To start, however, we illustrate the fundamental mechanism that leads to the singularity formation, by addressing a simulation which employed a reduced induction equation in which only the Hall term is considered. Physically, this case corresponds to the electron MHD regime with a massless electron fluid and a background of resting ions, and its evolution is completely described by the Burgers equation for β .

FIG. 1 shows plots of the toroidal magnetic field component, b_φ , and the radial component of the electron velocity, $v_{e,r}$, which, in this reduced system, is proportional to the corresponding current density component $j_r = -\rho_0 v_{e,r}/d_i$, for a run with $d_i = 0.2$. From these plots, the mechanism of current sheet formation becomes obvious: On lines $r = \text{const}$, the profile of b_φ is transported parallel to the z -axis while it steepens to, eventually, form a sharp edge. This edge corresponds to a highly localized current distribution $j_r = -\partial_z b_\varphi$, which in the electron MHD case results from the electron motion alone. The temporal evolution of $\max(|j_r|)^{-1}$, where the maximum is taken over the entire domain $[-2, 2] \times [0, 2]$, together

with the corresponding values obtained from the analytical Burgers-solution are included in FIG. 2. Evidently, the analytical solution is well reproduced by the computations.

Returning to the full Hall-MHD system, the time histories of $\max(|j_r|)^{-1}$ for the three simulations with fixed $d_i = 0.2$ and initial velocity amplitudes of $\hat{v} = -5, 0$ and 5 , respectively, are shown in FIG. 2. For comparison, the electron MHD run ($d_i = 0.2$) discussed above is also included. In all three cases, the maximum current density finally grows without indication of saturation and with a growth behavior of at least $1/(t - t^*)$, i.e. a finite time-singularity. The earlier stages of the runs, however, exhibit characteristic differences: With $\hat{v} = 0$, i.e. initially resting ions, the growth is roughly similar to the pure electron MHD case, with a slightly slower onset and a faster increase of $\max(j_r)$ after $t \approx 0.25$. Here, the ion fluid is gradually accelerated by the electromagnetic forces, and its motion contributes to magnetic flux transport through the convective electric field. In the case of $\hat{v} = 5$, the growth sets in even earlier, leading directly to what seems to be a singularity at around $t \approx 0.22$. Here, the generalized ion vorticity is zero, so that the second condition in Eq. (16) is clearly satisfied. For $\hat{v} = -5$, on the other hand, the initial ion motion counteracts the Hall term induced flux transport in positive z -direction close to the z -axis. Here, we observed a rather involved flow pattern resulting from the initial convection and the magnetic forces: The plasma is accelerated radially inward and along the negative z -direction, gets repelled from the z -axis by the increasing thermal pressure and forms a MHD-like slow shock structure. Despite this strong dynamical behavior, a thin sheet starts to form close to the z -axis at $z \approx 0.75$ and dominates, by amplitude the other current structures related to the MHD-like evolution, after $t \approx 0.5$. The signature of this current sheet is observed in the magnetic field and becomes more obvious in the close-up plot of the radial electron velocity (FIG. 3). Thus, even though condition (16) isn't met by the initial condition, the small scale structures form in the course of the plasma dynamics and finally collapse in finite time.

FIG. 4 and 5 further illustrate the singularity formation for the case $d_i = 0.2, \hat{v} = 0$ in terms of the profiles of b_φ and the radial electron velocity component, $v_{e,r}$ at radius $r = 0.034$. The steepening of the magnetic field profile during its convection along z is obvious from these cuts. At the same time, the electron current density blows up, and its maximum at $t = 0.3121$ is 30, which is ≈ 75 times the initial maximum value. Also visible is the formation of a dip in the b_φ -profile trailing behind the steepening gradient. This minimum is associated with a local inversion of the plasma density gradient at the singularity locus

and can be interpreted as an effect of plasma compressibility.

The second set of simulation runs involves the variation of the ion skin depth d_i for the same initial conditions with $\hat{v} = 0$, i.e. resting ions. In addition to the previous value of $d_i = 0.2$, we used $d_i = 0.05$ and $d_i = 0$, where the latter case corresponds to the pure MHD dynamics. Plots of the growth of $\max(1/j_r)^{-1}$ are given in FIG. 6. Comparing the cases $d_i = 0.2$ and $d_i = 0.05$, we find similar behavior, but a later singularity time in the $d_i = 0.05$ case. In addition, the behavior at $t \approx 0.78$ deviates from the strict form $1/(t - t^*)$ which coincides with strong signatures in the ion dynamics, i.e. the ion velocity and mass density, that stem from the ion response to the current sheet. However, these signatures appear smooth and have larger length scales than the signature in the current density, and no clear indication of a suppression of the singularity tendency could be found here. Finally addressing the pure MHD run with $d_i = 0$, the data show significant growth of the current density as well. A logarithmic fit to the current density (now shown here) reveals exponential growth between $t = 1$ and $t \approx 1.4$, and the simulation data show the formation of a current sheet in conjunction with compressible shocks that form on the leading edges of diverging plasma flows along the z -axis. Thus, the behavior in this case is definitively different from the singularities found in the Hall-MHD cases.

IV. SUMMARY

In this paper, we have demonstrated the tendency towards finite time singularities in axisymmetric Hall-MHD configurations. The underlying fundamental mechanism was identified to be the electron dynamics described by the Hall term in Ohm's law which in this geometry leads to a Burgers like structure of the induction equation. Using numerical simulations of the complete Hall-MHD equations it could be shown that this mechanism is generic for a wide class of initial conditions. The potential to create small structures on short time scales demonstrates the relevance of the Hall term in collisionless plasma system for many settings like fast magnetic reconnection or filamentation processes [24].

Acknowledgments

This work was supported by the INTAS program under project number 00292. The work of J.D. and R.G. was supported by SFB 591 of the Deutsche Forschungsgesellschaft. The work of V.R. was also supported by RFBR, by the Russian State Program for Support of the Leading Scientific Schools, and by the Russian Science Support Foundation.

- [1] C. L. Fefferman, *Existence & smoothness of the navier-stokes equation*, Clay Mathematics Institute
http://www.claymath.org/prizeproblems/navier_stokes.pdf (2000).
- [2] U. Frisch, T. Matsumoto, and J. Bec, *J. Stat. Phys.* **113**, 761 (2003).
- [3] R. M. Kerr, *Phys. Fluids A* **5**, 1725 (1993).
- [4] R. B. Pelz, *J. Fluid. Mech.* **444**, 299 (2001).
- [5] R. Grauer, C. Marliani, and K. Germaschewski, *Phys. Rev. Lett.* **80**, 4177 (1998).
- [6] R. Grauer and C. Marliani, *Phys. Rev. Lett.* **84**, 4850 (2000).
- [7] Z.-S. She and E. Leveque, *Phys. Rev. Lett.* **72**, 336 (1994).
- [8] B. Dubrulle, *Phys. Rev. Lett.* **73**, 959 (1994).
- [9] R. Grauer, J. Krug, and C. Marliani, *Physics Lett. A* **195**, 335 (1994).
- [10] H. Politano and A. Pouquet, *Phys. Rev. E* **52**, 636 (1995).
- [11] E. Balkovsky, G. Falkovich, I. Kolokolov, and V. Lebedev, *Phys. Rev. Lett.* **78**, 1452 (1997).
- [12] W. E. and E. V. Eijnden, *Phys. Rev. Lett.* **83**, 2572 (1999).
- [13] M. Lässig, *Phys. Rev. Lett.* **84**, 2618 (2000).
- [14] J. Birn, J. F. Drake, M. A. Shay, B. N. Rogers, R. E. Denton, M. Hesse, M. Kuznetsova, Z. W. Ma, A. Bhattacharjee, A. Otto, et al., *Journal of Geophysical Research* **106**, 3715 (2001).
- [15] M. Shay, J. Drake, B. Rogers, and R. Denton, *J. Geophys. Res.* **106**, 3759 (2001).
- [16] H. E. Petschek, in *Physics of solar flares*, edited by W. N. Hess, Washington, DC, (1964), vol. 50 of *NASA SP*, pp. 425–439.
- [17] U. Frisch, A. Pouquet, P. L. Sulem, and M. Meneguzzi, *J. Méc. Théor. Appl.* **Numéro spécial**, 191 (1983).
- [18] A. S. Kingsep, K. V. Chukbar, and V. V. Yan'kov, Consultants Bureau, New York, (1990),

vol. 16, pp. 243–291.

- [19] D. Biskamp, E. Schwarz, and J. F. Drake, *Phys. Rev. Lett.* **76**, 1264 (1996).
- [20] V. P. Ruban, *Phys. Rev. E* **65**, 047401 (2002).
- [21] V. Ruban and S. L. Senchenko, *Physica Scripta* **69** 227 (2004).
- [22] D. Biskamp, E. Schwarz, and J. F. Drake, *Phys. Plasmas* **4**, 1002 (1997).
- [23] J. Dreher and R. Grauer, *Parallel Computing* (in 2005), in press.
- [24] D. Laveder, T. Passot, and P. L. Sulem, *Phys. Plasmas* **9**, 293 (2002).

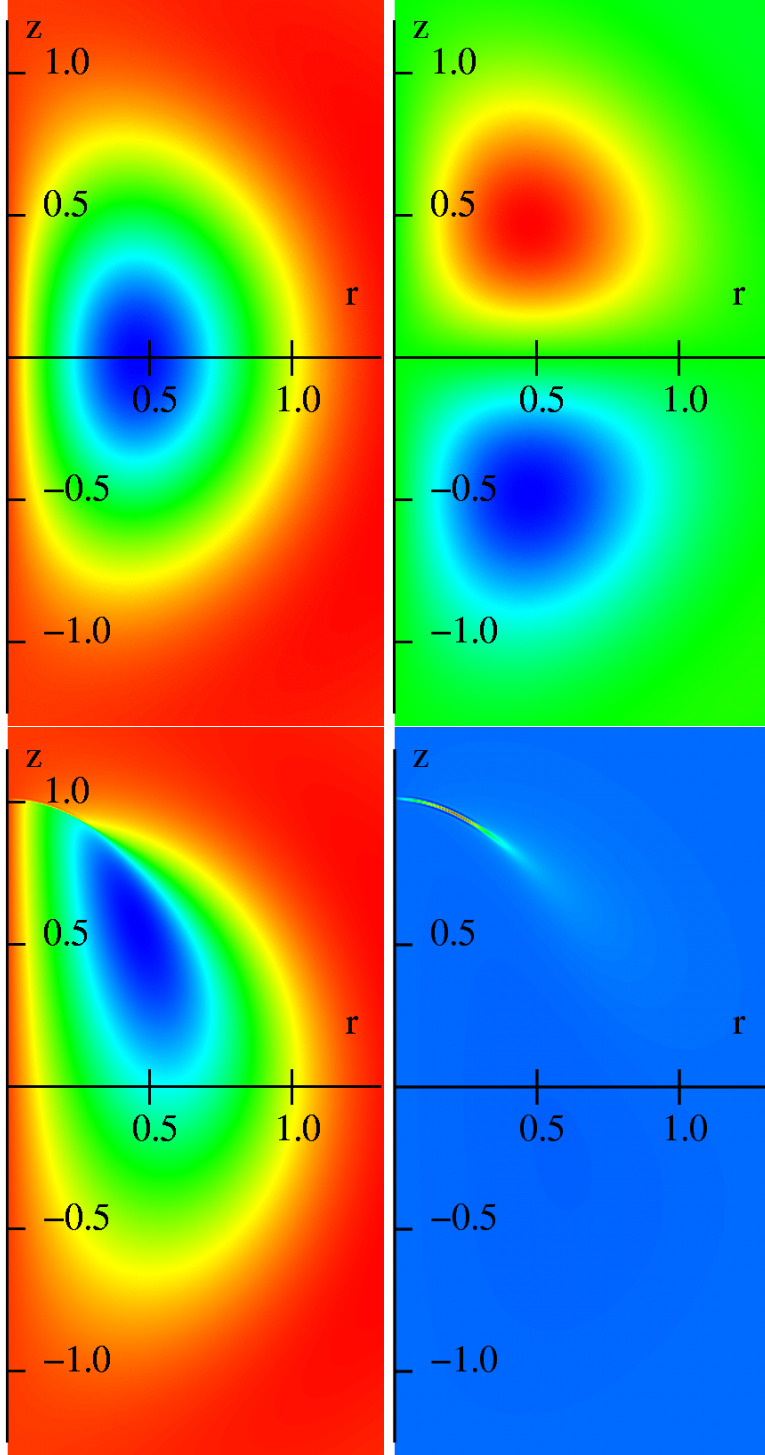


FIG. 1: Plots of the toroidal magnetic field b_φ (left) and the radial electron velocity component (right) at times $t = 0$ (upper) and $t = 0.35$ (lower) for the electron MHD run. The steepening of the b_φ -profile corresponds to current sheet formation. Ranges of b_φ are $[-1.27, 0.081]$ at both times (colors blue to red), while the electron velocity starts with $[-0.39, 0.39]$ at $t = 0$ and grows to $[-0.25, 3.95]$ at $t = 0.35$.

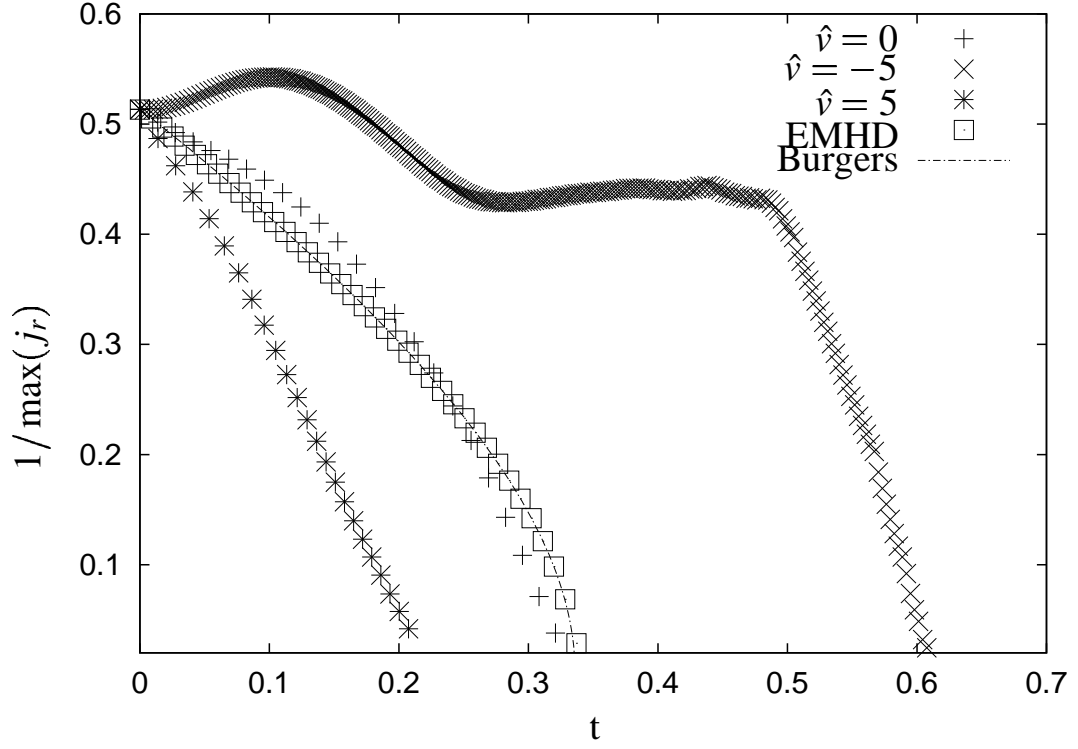


FIG. 2: Time evolution of $\max(|j_r|)^{-1}$ for Hall-MHD runs with $d_i = 0.2$ and $\hat{v} = -5, 0$, and 5 , respectively. Also shown is the Electron-MHD run (squares) together with the corresponding analytical solution (line).

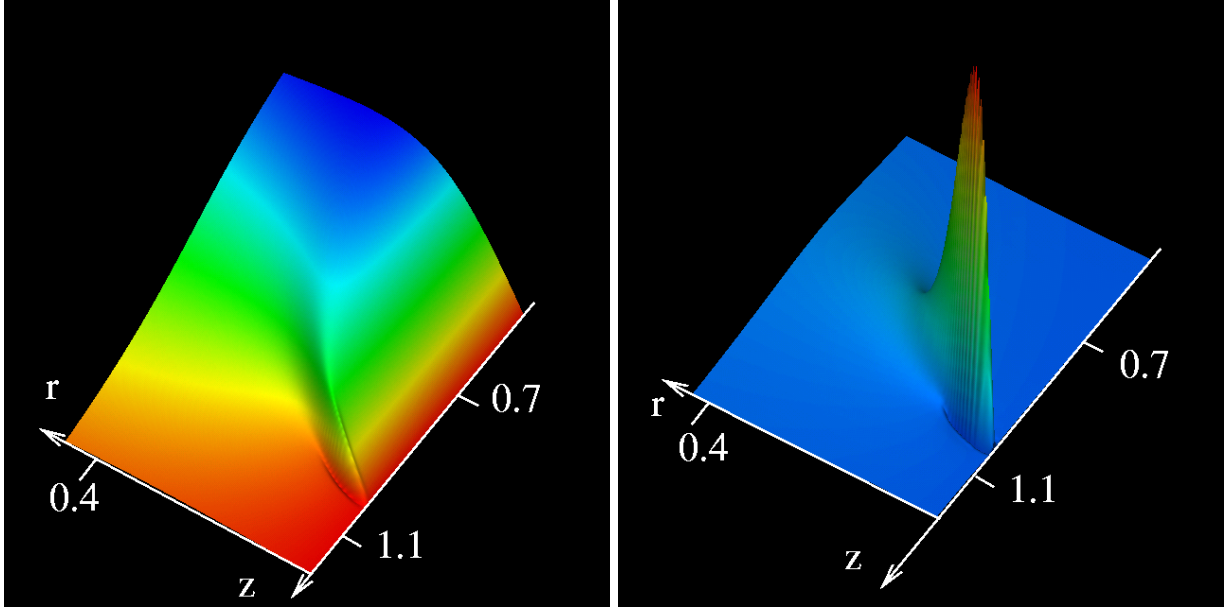


FIG. 3: Magnetic field, b_ϕ , (left) and radial electron velocity component, $v_{e,r}$ (right) at time $t = 0.6$ for the run with $d_i = 0.2$, $\hat{v} = -5$. The negative z -direction is to the right, positive r to the left.

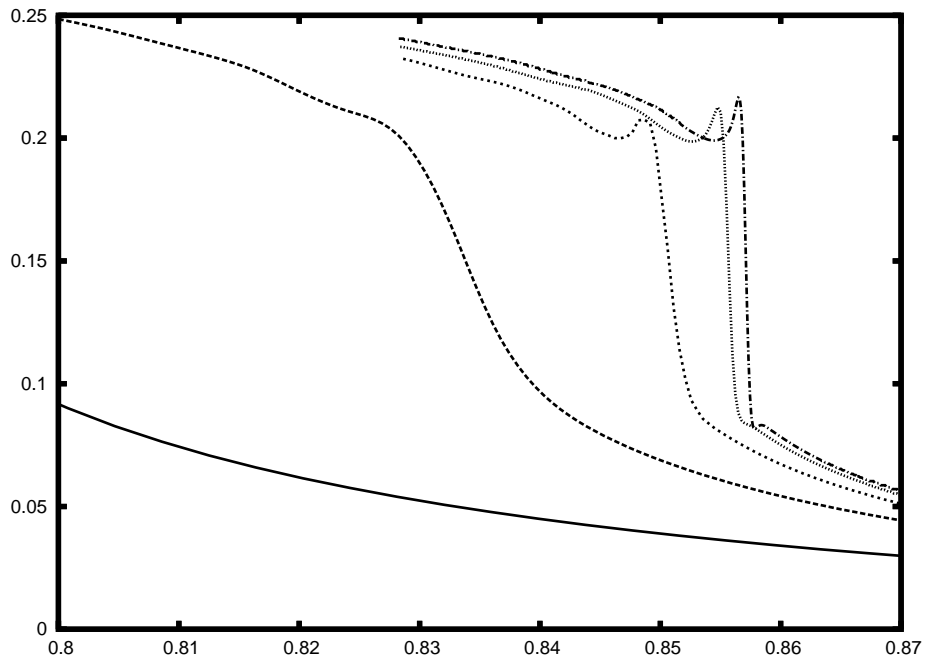


FIG. 4: b_φ vs. z at $r = 0.034$ and times $t = 0.276$ (solid), 0.2977 , 0.3084 , 0.3113 and 0.3121 respectively, for the run with $d_i = 0.2$, $\hat{v} = 0$. The curves illustrate the shock-like steepening of b_φ in time. Note that the computational domain covers $z \in [-2, 2]$.

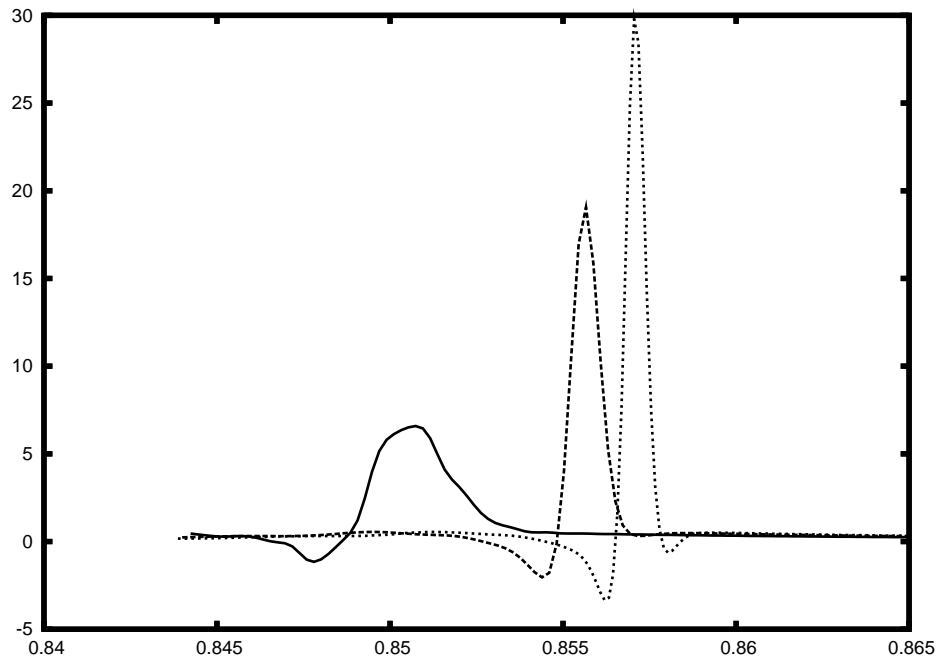


FIG. 5: Electron velocity component v_{er} vs. z at $r = 0.034$ and times $t = 0.3084$ (solid), 0.3113 and 0.3121 respectively, for the run with $d_i = 0.2$, $\hat{v} = 0$. The initial maximum of v_{er} is 0.39 .

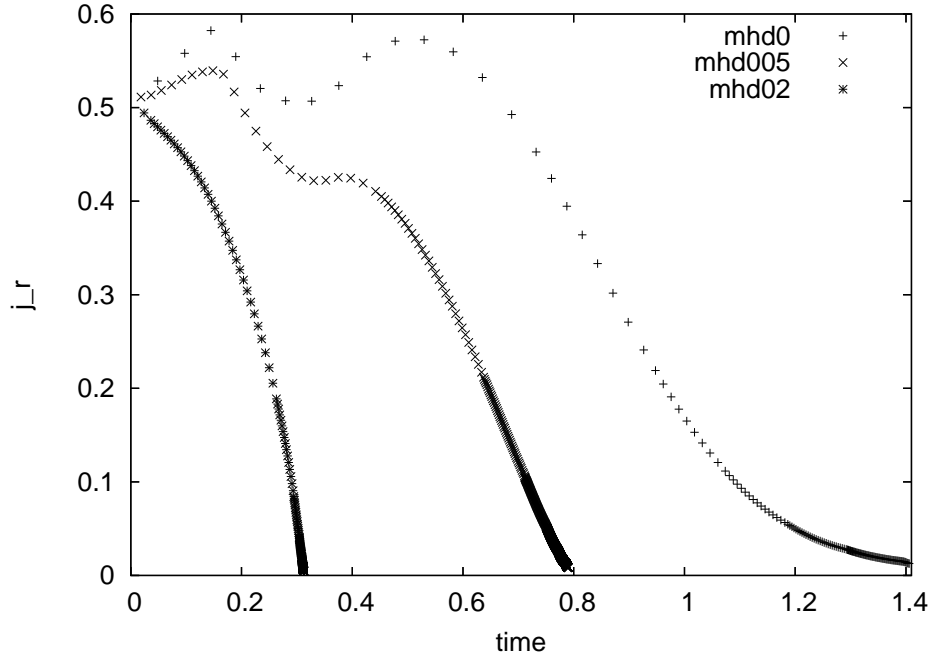


FIG. 6: Growth of $\max(|j_r|)$ for runs with $\hat{v} = 0$ and $d_i = 0$ (MHD), 0.05 and 0.2, respectively.